Development of Lightweight X-Ray Mirrors for the Constellation-X Mission

William W. Zhang, David A. Content, John P. Lehan, Robert Petre, and Timo T. Saha
NASA's Goddard Space Flight Center, Greenbelt, MD 20771 USA
Mikhail Gubarev, William D. Jones, and Stephen L. O'Dell
NASA's Marshall Space Flight Center, Huntsville, AL 35812 USA

ABSTRACT

The Constellation-X mission's Spectroscopic X-Ray Telescopes (SXT) [1] require an angular resolution of 15″ half-power diameter (HPD) with extremely lightweight grazing incidence mirrors. The areal density of the mirror must be about 1 kg/m^2 or less. In comparison with the state of the art X-ray mirrors represented by the XMM/Newton telescopes, this is approximately an order of magnitude less in mass areal density while maintaining the same angular resolution. We use a precision glass forming technique to fabricate mirrors that are 0.4mm thick and optical metrology to demonstrate that these mirrors can meet the stringent figure and micro-roughness requirements of the Constellation-X mission. We expect in the next few years to significantly improve the production yield and mirror quality to meet the goal of the mission, which is 5″ HPD for two reflections at the same mass.

Keywords: X-ray optics, lightweight optics, Constellation-X, space optics

1. INTRODUCTION

Combining the scientific desirability and practical factors of mirror making, a mirror for spaceflight applications can be characterized by three factors. The first factor is, of course, its angular resolution. As far as the typical astronomer is concerned, the finer the angular resolution is, the more scientifically useful and capable it is. The ultimate limit in this regard is the diffraction limit. The second factor comes from the spaceflight requirement: the mirror has to be as lightweight as possible because of the significant cost of launching any mass into space. In the case of X-ray mirrors, this translates to the requirement that the mirror must be very thin. The third factor is financial, i.e., the production cost of these mirrors should be low. Any mirror system for a spaceflight application is a compromise of these three factors. It has to be scientifically useful, can be launched into space, and has to be economically feasible to produce.

There is another important factor that is a combination of the latter two of the three fundamental factors, i.e., the total photon collection area. To the extent that the mirror production cost is low, thereby more of it can be fabricated, and to the extent that the mirror is light so that a given launch capability can launch more of it into space, one can have more photon collection area. The astronomer always prefer a larger photon collection area as long as the angular resolution remains the same.

In the past 40 years, various techniques for fabricating X-ray mirrors have been developed and used successfully to one degree or another. They can be broadly classified into two categories: grinding-and-polishing, and replication. In the grinding-and-polishing category belong the mirrors on Einstein [2], ROSAT [3], and Chandra [4], whereas in the replication category the mirrors on EXOSAT [5], XMM/Newton [6] and Astro-E2 [7]. The grinding-and-polishing technique is capable of fabricating mirrors with exquisitely high angular resolutions. But such fabricated mirrors are very massive and the fabrication process very expensive. On the other hand, the replication technique has produced some of the lightest mirrors that have ever flown. Its main shortcoming is that their angular resolution is poor. For example, the Astro-E2 mirror holds the

Optics for EUV, X-Ray, and Gamma-Ray Astronomy II, edited by Oberto Citterio, Stephen L. O'Dell,
Proc. of SPIE Vol. 5900, 59000V, (2005) · 0277-786X/05/$15 · doi: 10.1117/12.614462

record of being the most lightweight at an areal density of only 0.3 kg/m^2, but its angular resolution is only ~110″ HPD for two reflections. The XMM/Newton mirrors, on the other hand, has a typical areal density of ~7 kg/m^2 and achieves an angular resolution of 15″ HPD for two reflections.

In the replication category there are at least three different techniques. They share the same goal of copying the figure and micro-roughness of ground-and-polished mandrels to very thin substrates. These substrates or mirrors are then aligned and integrated. The first replication technique was the epoxy replication technique developed and used for the EXOSAT mirrors. It achieved an angular resolution of 18″ HPD for two reflections. The second technique was the Ni electroforming technique that was pioneered in the 1960's by various groups and culminated in the production of the XMM/Newton mirrors which have an angular resolution better than 15″ HPD for two reflections. The Astro-E2 mission resurrected the epoxy replication technique and used it for the first time to make segmented X-ray mirrors.

In recent years the technique of thermally forming thin glass sheets has been developed to make segmented X-ray mirrors. As far as we know, the trend started with Labov [8] who used a machined concave stainless steel mold to form thin glass sheets to focusing X-ray mirrors. The reason for using the concave mold was so that the X-ray reflecting surface is not in contact with the mold surface which typically has numerous tool marks. He achieved an angular resolution of 2 to 3 arc-minutes HPD for two reflectrions. In the 1990's Craig et al. [9] used the same technique. They also achieved arc-minute mirrors.

In the last several years, under the auspices of the Constellation-X project, we have been developing a slumping technique that uses convex mandrels [10, 11].

2. MIRROR FABRICATION

Figure 1 illustrates the mirror forming process. A flat sheet of Schott D263 glass, 0.4mm thick, is placed on the side of a horizontally placed Wolter-I mandrel, either parabolic or hyperbolic. Then the mandrel and the glass sheet are heated slowly in a specially designed oven for temperature uniformity to about 600°C. In the course of this temperature ramp-up, the glass sheet slowly slumps under its own weight and wraps itself around the nearly cylindrical mandrel. Then the mandrel and glass sheet are cooled slowly to ensure that they are close to temperature equilibrium at any given time to ensure that the glass sheet, now having the shape of a Wolter-I mirror, has as a small residual stress as possible when reaching room temperature.

The glass sheet slumping process is controlled by its temperature and its weight. As such, the edges of the formed mirror are almost always the worst part of the mirror. Therefore we perform a post-forming trimming to remove about 0.5 to 1 inch near the edge of the entire mirror. In practice, we use a template for this trimming process to ensure that the resultant mirror meets certain dimensional requirements for the purpose of alignment and integration into the assembly.

For the purpose of this technology development, the mirror produced typically has a radius of curvature around 250mm. Its axial height/length is 200mm, and covers 50° in the azimuthal direction.

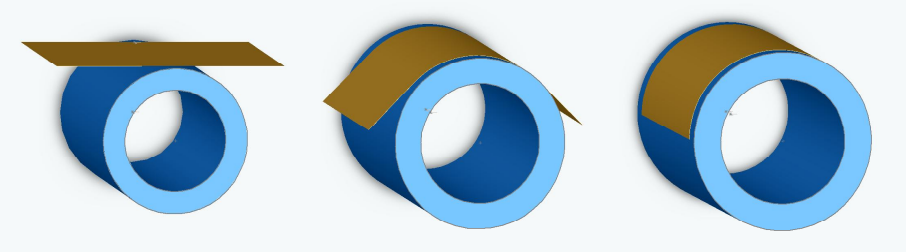

Figure 1. An illustration of the mirror forming process. The whole process takes place inside an electric oven meeting stringent temperature uniformity requirements.

3. VERIFICATION METROLOGY

The mirror fabrication process does not depend at all on any metrology. This feature is, of course, part of the reason why the replication process is an inexpensive one. But for the purpose of technology development, verification metrology is essential in giving feedback to the replication process. In this section, we first outline the mathematical aspects of the requirements imposed on the mirror, then we will show how to measure each aspect of the mirror, and finally present the measurement result that represents the status of the current technology development.

3.1 Mathematical Description of the Mirror

For convenience and ease of visualization, the standard Wolter-I prescription of a mirror, either parabolic or hyperbolic, can be generalized and written as

$$\rho(z,\phi) = \rho_0(\phi) + z\cdot\tan\theta(\phi) - \left(\frac{2z}{L}\right)^2 \cdot s(\phi) + R(z,\phi), \qquad (1)$$

where $\rho^2 = \sqrt{x^2+y^2}$, in the coordinate system as defined in Figure 2. The segment mirror in the present context is defined in the region

$$-\frac{L}{2} \le z \le \frac{L}{2}, \qquad L = 200 \text{ mm; and } \; 0^o \le \phi \le 50^o.$$

For a practically perfect Wolter-I mirror, of course, all the dependence on azimuthal angle and the fourth term vanish. Eq. (1) describes a real-world mirror whose various errors can be defined and measured as follows.

AVERAGE RADIUS AND ROUNDNESS ERROR The first term in Eq (1) can be further rewritten as

$$\rho_0(\phi) = \rho_0 + \Delta\rho_0 + \Delta\rho(\phi), \qquad (2)$$

where ρ_o is azimuth-independent and represents the design radius; $\Delta\rho_o$, also azimuth-independent, represents the deviation from the design value; and $\Delta\rho(\phi)$, by definition, having a zero mean, represents the in-phase out-of-roundness.

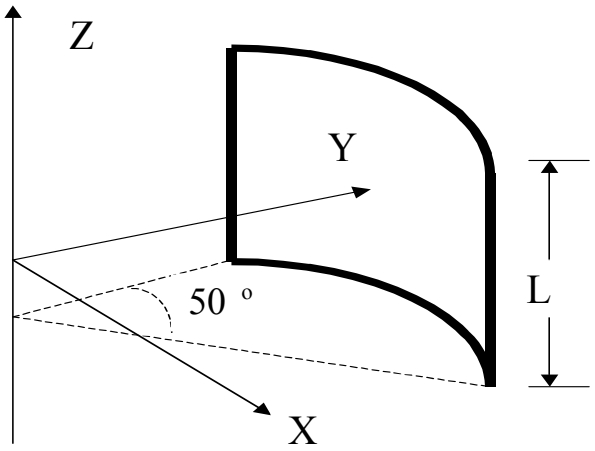

Figure 2. Coordinate system for the specification and measurement of the mirror.

AVERAGE CONE ANGLE ERROR AND CONE ANGLE VARIATION Similarly the cone angle in the second term in Eq. (1) can be rewritten as

$$\theta(\phi) = \theta_0 + \Delta\theta_0 + \Delta\theta(\phi), \qquad (3)$$

where θ_o is azimuth-independent and the design cone angle; $\Delta\theta_o$, also azimuth-independent, represents the deviation from the design value; and $\Delta\theta(\phi)$, by definition, having a zero mean, represents any cone angle variation as a function of azimuth.

AVERAGE SAG ERROR AND SAG VARIATION Similarly the sag term in Eq. (1) can also be rewritten as

$$s(\phi) = s_0 + \Delta s_0 + \Delta s(\phi), \qquad (4)$$

where s_o is azimuth-independent and the design sag; Δs_o, also azimuth-independent, represents the deviation from the design sag; and $\Delta s(\phi)$, by definition, having a zero mean, represents any sag variation as a function of azimuth.

AXIAL FIGURE ERROR The last term in Eq. (1), $R(z,\phi)$, represents the rest of the deviation of the real-world mirror from that of a mathematically perfect mirror. Again by definition, this term has a zero mean. It is important to note that the grazing incidence nature of the X-ray optics determines that the variation of $R(z,\phi)$ with z is much more important than its variation with azimuth angle ϕ. In other words, we can tolerate a much higher slope error in the azimuth direction than in the z direction. This difference in tolerance can be expressed as

$$\frac{\partial R(z,\phi)}{\partial z} \sim \frac{\alpha}{\rho_o} \cdot \frac{\partial R(z,\phi)}{\partial \phi}, \qquad (5)$$

where α is the grazing angle. Given the fact that in our mirror fabrication process the two independent directions are treated the same, we expect that the variations in the two directions are similar, if not identical. As such we only need to be concerned with the variation in z. Once the requirement on variation in the z direction is met, the variation in the azimuth direction is automatically also met.

Therefore it is only necessary to measure the $R(z,\phi)$ as a function of z at several or many different azimuths, in other words, many axial figure measurements. This is why this term is dubbed the axial figure error, even though it is dependent upon azimuth also.

3.2 Metrology Equipment

The mirror quantities defined in Eq. (2), (3), (4), and (5) cannot be measured with one piece of metrology equipment. The spatial extent and precision requirement can be met with three separate instruments.

A custom-designed and built cylindrical coordinate measuring machine (CCMM), as shown in Figure 3, has a precision of 0.1μm RMS over its work volume. It can adequately measure the radius, cone angle, and the sag, i.e., those quantities defined in Eq. (2), (3), and (4). It typically samples the mirror surface every 0.5mm. The right-side panel of Figure 3 shows a typical measurement result from this machine. The map represents the residual deviation of the mirror from a fit cone. The cone angle and the average radius of the fit cone are in nominal agreement with those of the mandrel used for creating this mirror. The map has several features. The first one is the nearly symmetric left and right lobes separated by the bluish region centered at about 30^o azimuth. The second one is that the lobes, as indicated by the color coding, are bulging toward larger radii, indicating that the mirror does have a more or less Wolter-I axial curvature. The third feature is that only the axial sag near the 30^o azimuth is reasonably close to the specifically required sag, namely 1.1μm, in this case. Sags in other azimuths are all too large.

Numerous experiments have demonstrated that this pattern is mainly due to gravity distortion. During measurement this mirror was supported in nearly the vertical direction at two points at the bottom and a single point at the top, close to a kinematic mount. The bottom two points are near 10^o and 40^o, respectively. The top point is at 29^o. We are in the beginning of modeling and understanding quantitatively this distortion. Eventually we will subtract this distortion to arrive at the figure of the mirror when it is in a gravity-free environment.

A commercial Fizeau interferometer, similar to the one shown in Figure 4, is used to measure the axial figure. The Fizeau interferometer, by design, outputs a plane wave, and as such is typically good for measuring flat or nearly flat mirrors. In our specific case of a nearly cylindrical mirror, only a sliver of the wave front is returned. This sliver along the optical axis direction gives the one-dimensional figure at the specific azimuth. The right-side panel in Figure 4 shows a map constructed of 27 axial scans of this kind. For each scan, a fit to the 2^{nd} order polynomial, i.e., the sag, is removed. The sag as a function of azimuth is plotted at the top panel. Two important features should be noted. The first one is that the average sag of the mirror is certainly in the vicinity of the correct number, i.e., 1.1μm. But the variation of sag as azimuth is relatively large. Again this is due to gravity distortion. The second feature is the near perfect left-right symmetry in the color-coded height error map. The three support points can be clearly made out: 10^o and 40^o at the bottom and 25^o at the top. Again the large-scale figure error in this case is dominated by gravity distortion.

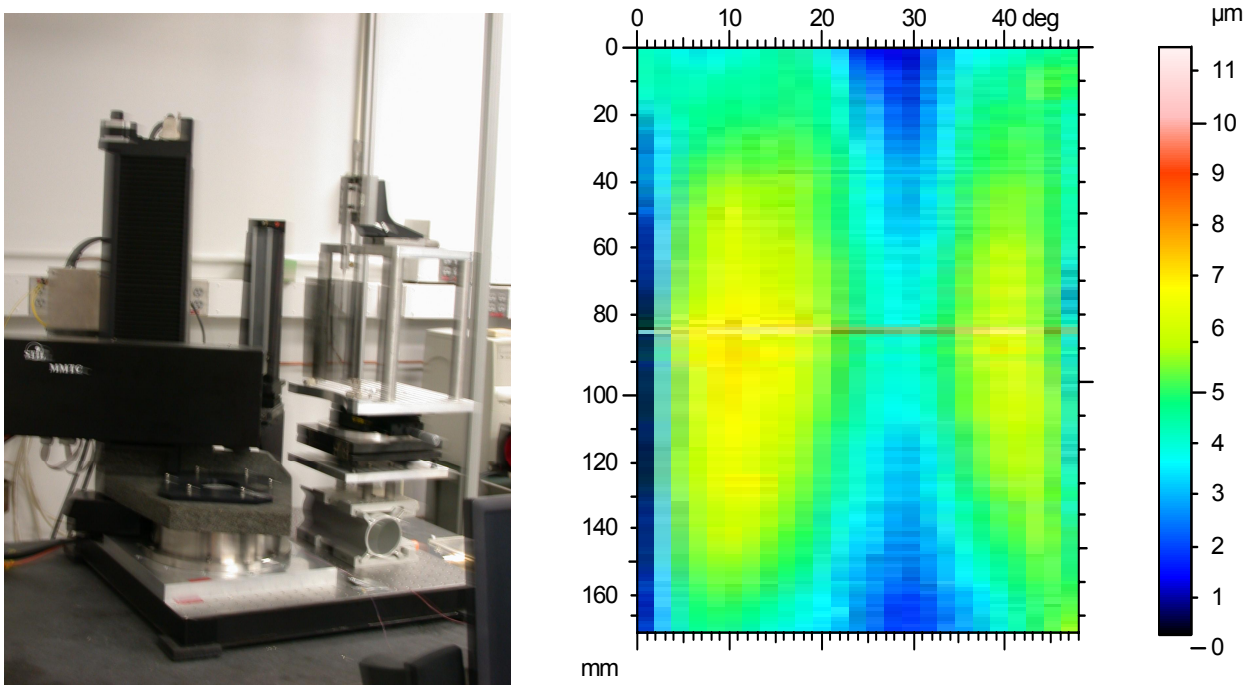

Figure 3. Left: A custom-designed and built (by STIL) cylindrical coordinate measuring machine. Right: a surface map generated of a mirror using this machine. In generating this map, a fit cone has been removed and color-coded residual shows the sag. The most obvious features in this map are due to gravity distortion**.**

Individual axial scans can be further analyzed to obtain detailed axial figure error. Figure 5 shows four typical axial scans. The notable features are: (1) that the mirror axial figure slope error is dominated by mid-frequency errors, i.e., those with spatial scales between a few millimeters and 20 millimeters; and (2) several "craters" or "holes" strongly indicate that they result from dust particles that were trapped or sandwiched between the mirror and the forming mandrel surface during the mirror forming process. A very direct and reasonable inference from this is that other much smaller and therefore less discernable holes are also a result of particles, albeit significantly smaller ones.

Equivalently these axial scans can be analyzed in the Fourier spatial frequency domain. Figure 6 shows such a plot, The ordinate shows the modified PSD which is normalized so that the integrated area under the curve is the square of the axial slope RMS (see Reference [10] for details). The purple straight line shows the nominal Constellation-X requirement. It is clear that the axial slope error is dominated by ripples in the spatial scales ranging from 3mm to 20mm. The figure error in the spatial scales ranging from 20mm to 200mm actually far exceeds the requirement.

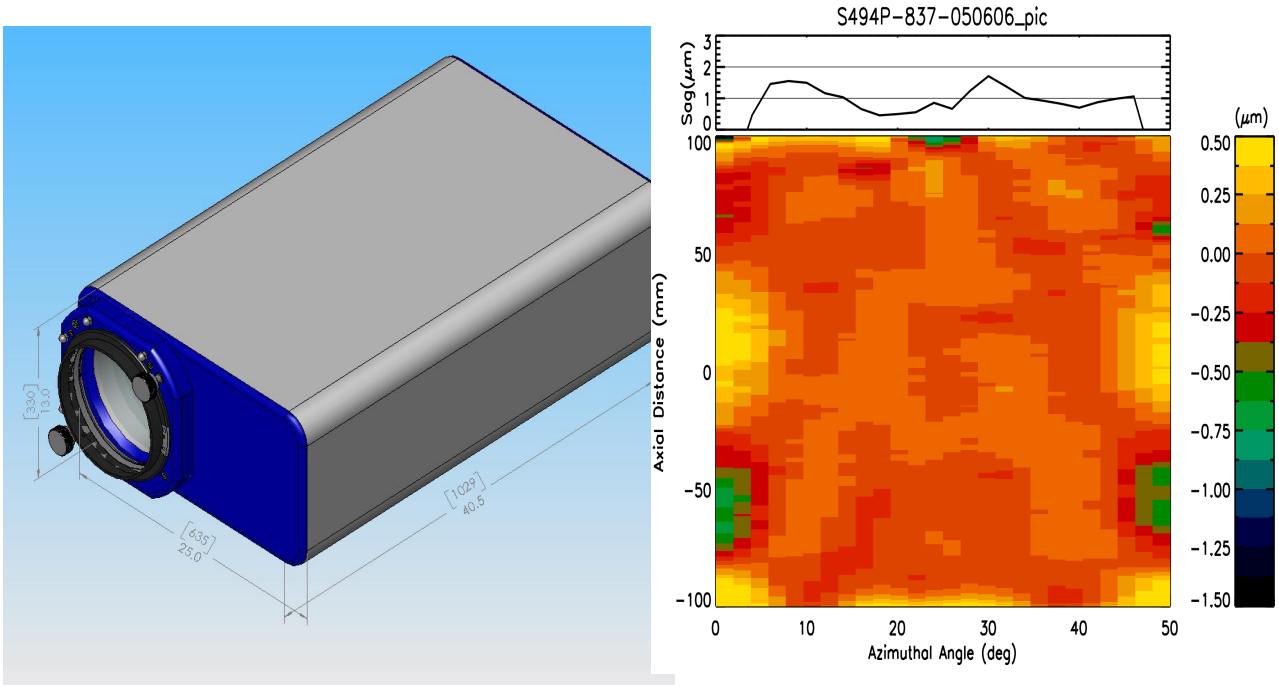

Figure 4. Left: An illustration picture of a Fizeau phase-measuring interferometer. It outputs a plane wave. Right: A map generated of a mirror using a Fizeau interferometer. It consists of 27 independent axial scans. The sag of each scan has been removed and plotted at the top panel.

Our Fizeau interferometer can only sample every 0.3 mm in the axial direction. As such it does not cover what is normally called the mirco-roughness. Another instrument, an interferometric profilometer, as shown in Figure 7, is used. It samples the mirror surface over an area of 0.6mm by 0.6mm. The right-side panel of Figure 7 shows a typical map obtained with this instrument. It is clear that the mirror still retains the float glass surface before slumping, as such its surface microroughness is very good, at about 3.2 Angstroms RMS, far exceeding the Con-X requirement of 5 Angstroms. In particular we note that the profilometer used for this measurement has its limit close to 3 Angstroms. It is possible, even likely, that the real surface is better than 3.2 Angstroms. This feature allows us to concentrate on improving the mirror figures without having to be concerned with the microroughness.

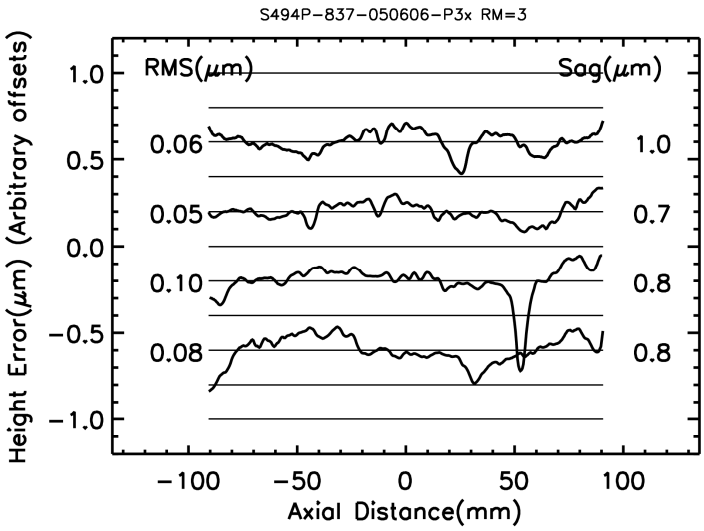

Figure 5. Four typical axial scans. The 2nd order, or sag has been removed for each scan. Its value is displayed on the right. The RMS variation is displayed at the left.

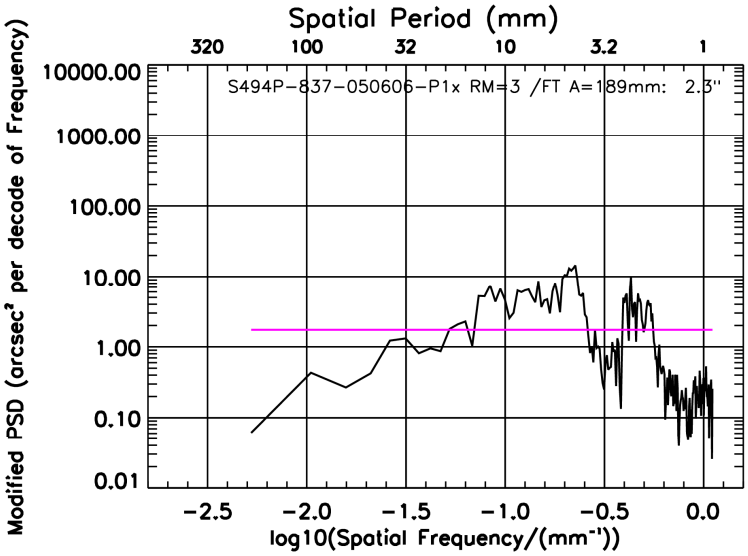

Figure 6. Axial scans similar to those in Figure 5, except that they are plotted in the Fourier frequency domain. The purple line represents the nominal Constellation-X requirement. The modified PSD is defined such that the square root of the area under a curve as plotted gives square of the axial slope RMS.

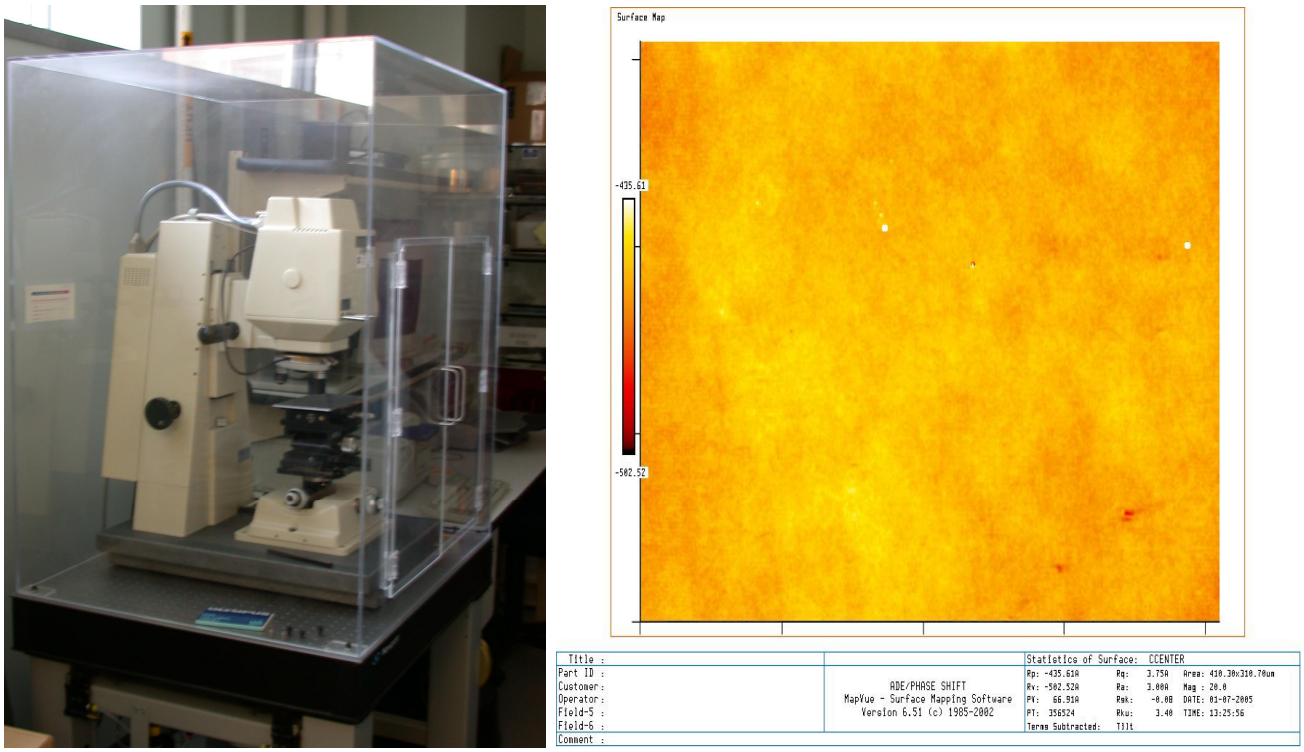

Figure 7. Left: Photograph of a WYKO surface profilometer. Right: The surface map of a mirror. Over an area of 0.6mm by 0.6mm it has an RMS roughness of 3.2 Angstrom.

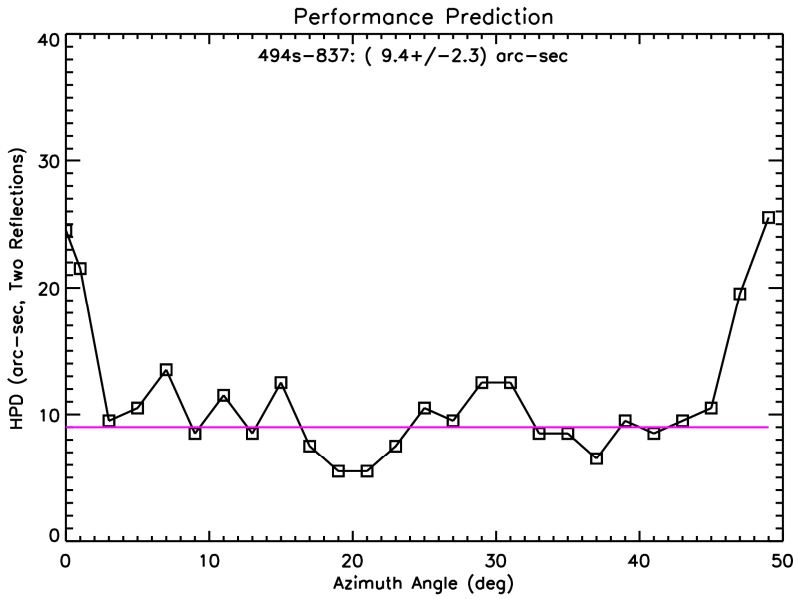

Figure 8. Performance prediction for a recently fabricated mirror. The purple line represents the nominal requirement of Constellation-X.

Figure 8 shows the performance prediction of a recently fabricated mirror at 1 keV with a grazing angle of 1.1°. The purple line represents the nominal requirement of the Constellation-X mission. It is clear that this mirror essentially meets the requirement, except for the few points near the azimuthal ends. In all likelihood, these points are caused by distortion of the mirror under gravity.

Table 1 is a scoreboard of our effort. All relevant parameters are listed. See Reference [12] for a discussion of these parameters in the context of the Constellation-X observatory. The developmental nature of our effort is evident in that several parameters are listed as P.E.R., meaning Probably Exceeded Requirement. These parameters are typically significantly influenced by gravity distortion and handling. We are in the beginning of modeling and understanding these effects.

Table 1. Constellation-X mirror development score board. This table contains all the parameters that are needed to characterize a mirror. The P.E.R. mean that we believe that they probably have exceeded the requirement, but we have not yet fully demonstrated it quantitatively because of gravity distortion and/or metrology capability at the present time.

Parameter (Unit)		Requirement*	Status**
Radius (μm)	Average ($\Delta\rho_o$)	< 10	P.E.R.
	Variation ($\Delta\rho(\phi)$)	< 2	P.E.R.
Cone Angle (arc-second)	Average ($\Delta\theta_o$)	< 1	P.E.R
	Variation ($\Delta\theta(\phi)$)	< 0.5	P.E.R.
Axial Sag (P-V) (μm)	Average (Δs_o)	< 0.1	P.E.R.
	Variation ($\Delta s(\phi)$)	< 0.1	P.E.R
Axial Slope	Figure: 200mm-20mm (arc-seconds)	< 1.3	1.0
	Mid-Frequency: 20mm-1mm (arc-seconds)	< 1.5	2.0
	Micro-roughness: 1mm-1μm (Angstrom)	< 5.0	3.2

*These requirements are for an observatory level image performance of 15" half-power diameter after two reflections. ** P.E.R. stands for Probably Exceeded Requirement

4. PROBLEMS AND PROSPECTS

Although we have essentially demonstrated that this technology can meet, very likely can exceed, the Constellation-X requirement, it is clear that there are several problems that we need to overcome before we can significantly improve the quality of the mirror. The first one is the metrology problem. Although, as of the writing of this paper, we have essentially all the necessary metrology equipment to measure all the quantities we need to measure, we have not yet quantitatively understood the gravity distortion and handling distortion. These distortions are currently dominating the large scale figure error, radius, sag, etc. Fortunately these problems can be overcome with standard finite element analyses. The straightforward iterative procedure is to compare FEM modeling results and real measurements to reconcile any difference. Once the model is understood and verified, we can back out the true figure of the mirror by subtracting the model from the real measurement.

The second significant problem is the mid-frequency errors, i.e., those slope errors with spatial scales from several millimeters to 20 millimeters. They are clearly caused by dust particles trapped between the mandrel

surface and glass sheet during the slumping process. The way to solve this problem is to slump in a totally clean environment. The truly clean environment is, of course, a vacuum. We will pursue funding to procure a vacuum oven to solve this problem once and for all.

Once these two problems are addressed, we will essentially be copying the forming mandrel with a very high degree of fidelity. We expect to be able to fabricate mirrors to the limit of the current mandrel quality: 7 arc-seconds HPD for two reflections. The door will be wide open for us to reach the goal of the Constellation-X mission, which is 5 arc-seconds HPD for two reflections.

5. ACKNOWLEDGEMENTS

The work reported here results from the hard work of many people at several institutions and companies. While it is not possible to list all their names, we would like to especially acknowledge the contributions of James Mazzarella, Marton Sharpe, David Colella, Melinda Hong, and Theo Hadjimichael. Their dedicated technical support has been indispensable in achieving the results reported here. This work has been financially supported in part by NASA through the Constellation-X Project Office at the Goddard Space Flight Center and through an Astronomy and Physics Research and Analysis (APRA) grant.

REFERENCES

1. N.E. White and H. Tananbaum, "Constellation-X Mission: Science Objectives and implementation Plan", SPIE Proc., vol. 4851, 293 (2003).
2. P.S. Young, 'Fabrication of the High Resolution Mirror Assembly for the HEAO-2 X-ray Telescope," SPIE Proc. Vol. 184, p. 131 (1979)
3. B. Aschenbach, "Design, construction, and performance of the ROSAT high resolution x-ray mirror assembly," Appl. Opt. Vol. 27, p. 1404 (1988)
4. L. P. van Speybroeck, et al., "Performance expectation versus reality," SPIE Proc. Vol. 3113, p. 89 (1997)
5. P. A. J. de Korte, "High-throughput replica optics," Appl. Opt. Vol. 27, p. 1440 (1988)
6. O. Citterio, et al., "Results of X-ray measurements on electroformed mirror shells for the XMM project," SPIE Proc. Vo. 1742, p.256 (1993)
7. Y. Soong, et al., "Conical thin foil x-ray mirror fabrication via surface replication," SPIE Proc., Vol. 2515, p. 64-69 (1995).
8. S. E. Labov, "Figured grazing incidence mirrors from reheated float glass." Appl. Opt. Vol. 27, P. 1465 (1988)
9. W. Craig, et al., "Hard x-ray optics for the HEFT balloon-borne payload: prototype design and status," SPIE Proc. Vol. 3445, p. 112 (1998)
10. W. Zhang, *et. al*., "Development of mirror segments for the Constellation-X Observatory", SPIE Proc., vol. 5168, 168 (2004).
11. W. Zhang, et al. "Hard x-ray optics for the HEFT balloon-borne payload: prototype design and status," SPIE Proc. Vol. 5488, p. 820 (2005)
12. W. Podgorski, et al. "Hard x-ray optics for the HEFT balloon-borne payload: prototype design and status," SPIE Proc. Vol. 5168, p. 239 (2004)